PAPER

Cu$_{2+1}$O/graphene nanosheets supported on three dimensional copper foam for sensitive and efficient non-enzymatic detection of glucose†

Liang Yang, [ID] Daoping Liu, Guomin Cui* and Yingming Xie

In situ growth of Cu$_{2+1}$O (Cu$_2$O with metal excess defects) was achieved through a facile hydrothermal process by employing porous Cu foam (CF) as substrate and the precursor, meanwhile, graphene nanosheets (GN) were deposited onto the Cu$_{2+1}$O/Cu foam substrate. The GN/Cu$_{2+1}$O/CF hybrid electrode provides a large accessible surface area, and contact between GN/Cu$_{2+1}$O and current collector (Cu foam) with good conductivity facilitated electron/ion transport. When being used as a potential biosensor for nonenzyme glucose detection, cyclic voltammetry (CV) and amperometric electrochemical method to evaluate the electrocatalytic performance of GN/Cu$_{2+1}$O/CF, and the GN/Cu$_{2+1}$O/CF hybrid electrode exhibits multistage linear detection ranges with high sensitivity (3.076 mA mM^{-1} cm^{-2}) and the detection limit is 5 μM. Furthermore, the GN/Cu$_{2+1}$O/CF electrode also presented excellent repeatability, stability and reproducibility and selectivity. The design of GN/Cu$_{2+1}$O/CF hybrid electrode provided a useful strategy for design electrochemistry non-enzymatic biosensors.

Introduction

Diabetes is a common chronic disease resulting from insulin deficiency, and the blood glucose level is the main index for the diagnosis. The early diagnosis of diabetes mellitus as well as sensitive detection of physiological glucose level in the blood is very important to avoid diabetic emergencies.[1] Until now, blood glucose monitoring technologies such as optical spectroscopy,[2] chemiluminescence,[3] fluorescence[4] and electrochemical method[5] have been widely developed for glucose detection. Among these, electrochemical technique is one of the promising methods for glucose detection due to the advantages of high sensitivity, ease of operation and the low cost.

For enzyme-base electrochemical glucose detections, the glucose concentration can be monitored at sensors with glucose oxidase immobilization by the determination of the consumption of dissolved oxygen or the production of hydrogen peroxide.[6] Another type is enzyme-free glucose sensor which without the use of glucose oxidase and avoid the drawbacks such as the high cost and instability of enzyme. Transition metals (Ni, Cu) and their oxide (NiO, CuO) have been extensively used in non-enzymatic glucose sensing[7-9] attributed to the outstanding redox activities in electrochemical catalytic processes, and in conventional

fabrication process, the transition metals were prepared in the form of nanoparticle powder, and they are modified on an conductive substrate with the addition of the polymer-Nafion, however, polymeric binder is not active for glucose sensing, which may hinder the electrochemical catalytic sites, and thus influence the glucose sensitivity.[10] In addition, due to the increased charge transfer resistance from the polymer binder, the electrochemical performance would inevitably be influenced.[11,12] Therefore, it is promising to design and synthesis nanostructured material by *in situ* growth on substrate, and micro/nanostructured materials with multi-dimensionalities received much attention for glucose sensing due to the low cost and facile fabrication or posthanding.[13]

Metal foam with low density, high specific surface area, open-pore structures, high strength-to-weight ratio and excellent electrical conductivity has received much attention and been applied in catalysis,[14] supercapacitors[15] and sensor in which copper foam was prepared by electrochemical route and excellent electrochemical property for enzyme-free glucose sensing was obtained.[16] Similar research was also reported, in which Cu foam was decorated by CuO nanowires and exhibited excellent sensitivity.[13]

Graphene, a two-dimensional layer of graphite with sp^2-C arranged in a hexagonal lattice has captured remarkable attention due to its excellent physical and chemical properties, such as its good biocompatibility, thermal and electrical conductivities, excellent mechanical strength, and large surface areas.[17] With low noise level in biological reactions, graphene based nanohybrid is a good candidate for slight current signals detections in electrocatalytic oxidation of glucose.[18] In catalytic reactions, the active species can be modified by the supporting

Institute of New Energy Science and Engineering, School of Energy and Power Engineering, University of Shanghai for Science and Technology, Shanghai 200093, China. E-mail: cgm1226@163.com; Fax: +86 21 55272320; Tel: +86 21 55272320

material-graphene which resulted in the enhanced electro-catalytic activity. Thus, the fabrication of graphene based hybrid electrode is an effective strategy for glucose detection.

In this study, we fabricated $Cu_{2+1}O$/graphene nanosheets hybrid on Cu foam for enzyme free glucose sensing. By employing Cu foam (CF) as conductive scaffold and precursor of *in situ* growth $Cu_{2+1}O$ nanocubes through a facile hydrothermal method, and during the hydrothermal process, the 3D conducting scaffold were coated with graphene nanosheets (GN). With large surface area, the hierarchical porous structure of $GN/Cu_{2+1}O/CF$ hybrid electrode is beneficial for effective diffusion of the glucose molecular. The electrode displayed remarkable performances such as high sensitivity, excellent repeatability, stability and reproducibility and selectivity towards glucose detection in an alkaline solution.

Experimental

Materials and methods

Sodium hydroxide (NaOH), sodium chloride (NaCl), D-(+)-glucose, ascorbic acid (AA) and uric acid (UA) were purchased from Sigma-Aldrich. Graphite powders (C, Z98.0%) were supplied by Tianjin Guangfu Delicacy Chemical Research Institute. Copper foam (thickness of 1 mm) was bought by Tianjing kemiou Ltd Co (P. R. China). Ultrapure water (18.2 MΩ cm, Milli-Q) was used during all experiments.

Preparation of GN GN/Cu₂₊₁O/CF and Cu₂₊₁O/CF

Graphene oxide (GO) was prepared from graphite powder using Hummer's method.[19] Graphite is treated with strong oxidants, and large amount of O-functionalities are formed in the carbon nanosheets which induced the increase of the interlayer spacing. A 100 ml volume of GO dispersion (0.8 mg ml^{-1}) was introduced into a stainless steel autoclave (4590 Micro Stirred Reactor, ParrInstrument Company). $GN/Cu_{2+1}O/CF$ were prepared by a hydrothermal process in which refluxed a copper foam substrate in an aqueous graphene oxide solution at 180 °C in an autoclave for 5 h and cool down at room temperature, and then, the substrate was taken out and washed with deionized water, at last dried in air.

GO was reduced by conventional hydrothermal treatment at 180 °C, during which the inner pressure reached 9 bar.[20] The $Cu_{2+1}O/CF$ was prepared by the same hydrothermal process as the preparation of $GN/Cu_{2+1}O/CF$ except using the distilled water instead of GO solution.

Instrumentation and electrochemical measurements

Scanning electron microscopy (SEM) was performed on a JEOL JSM-7400F instrument operating at an acceleration voltage of 3 kV. X-ray diffraction (XRD) data were collected on a Bruker DAVINCI D8 ADVANCE diffractometer using Cu K radiation (λ = 0.15406 nm). Chemical state analysis was carried out by X-ray photoelectron spectroscopy (XPS) completed with Auger spectroscopy using a Thermo ESCALAB 250 spectrometer with an Al Kα radiation source (passing energy 30 eV). All binding energies were calibrated using the C 1s hydrocarbon peak at 284.60 eV. The electrochemical properties of catalysts were studied in a conventional three-electrode cell. A saturated calomel electrode (SCE, Hg/Hg₂Cl₂) with a salt bridge was used as the reference electrode, and a Pt sheet was utilized as the counter-electrode. All specific activities were normalised to the geometric surface area of the working electrode. Electrochemical tests were performed at room temperature using a potentiostat (bio-logic, France).

Results and discussion

Characterization

The morphological properties of $GN/Cu_{2+1}O/CF$ nanostructures were examined by SEM. As shown in Fig. S1,† the CF is a scaffold
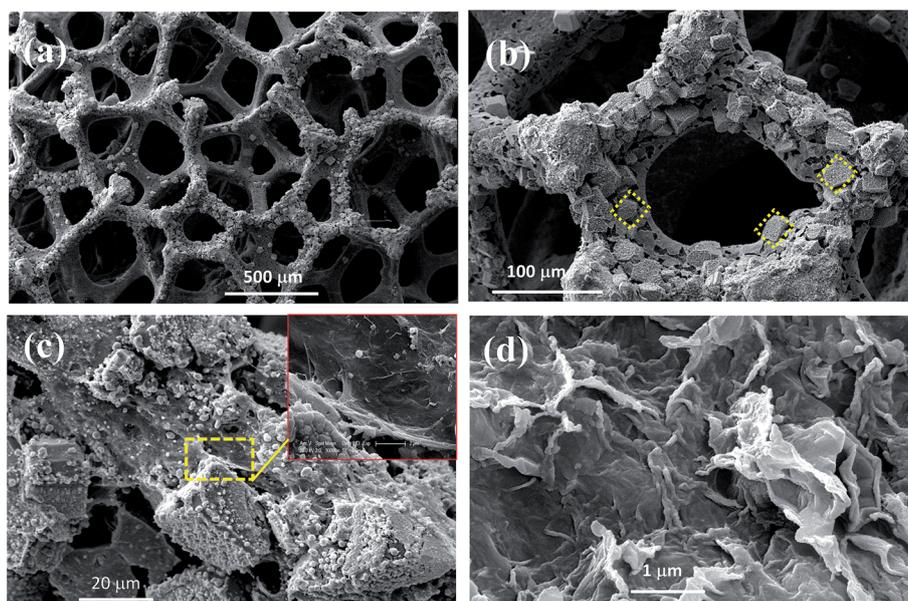

Fig. 1 SEM images of GN/Cu₂₊₁O/CF with (a) low and (b and c) high magnifications and the inset in (c) is the magnification image, (d) GN.
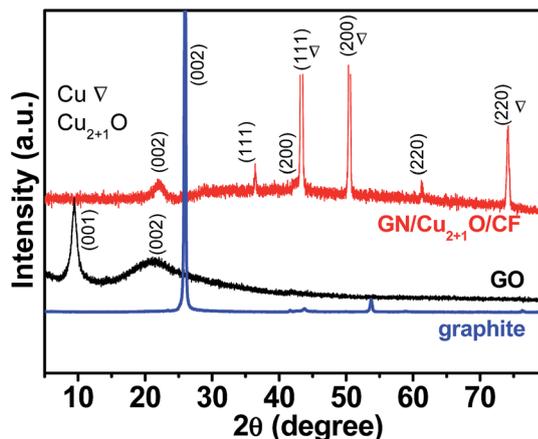
Fig. 2 XRD patterns of graphite, GO and GN/Cu$_{2+1}$O/CF.

with porous and continuous three dimensional structure, and the pore size ranged from 100 μm to 500 μm. Obviously Cu$_{2+1}$O with cubic morphology *in situ* grow on the surface of skeletons of the Cu substrate, and its surface roughness is remarkably enhanced compared with Cu foam (Fig. 1a and b). From Fig. 1b, Cu$_{2+1}$O with cubic morphology on the copper foam scaffold of can be observed. And the average edge-size of a cube was about 20 nm. The preparation of GN/Cu$_{2+1}$O/CF is a one-step hydrothermal process using GO solution as the solvent, so the formation of Cu$_{2+1}$O and reduction of GO occurred at the same time during the hydrothermal process. So we supposed that most of the graphene nanosheets are crosslinked with the Cu$_{2+1}$O nanocubes which can also be proved by the SEM image

in Fig. 1c. Fig. 1d presents the SEM image of GN after hydrothermal process, the layered structure of graphene nanosheets are not especially flat, but with folds and wrinkles on the surface which indicated the deformation during the exfoliation process.

XRD was used to investigate the structure and composition of the graphite and as-prepared GO, GN/Cu$_{2+1}$O/CF. In Fig. 2, we can found a sharp and strong peak at $2\theta = 26.265°$ which corresponds to the (002) plane (*d*-spacing: 0.339 nm) of pristine graphite sample. The diffraction peak at 9.5° corresponds to the (001) plane (*d*-spacing: 0.928 nm) of GO, and the negative shift angle of diffraction peak indicating the oxidation of graphite. Furthermore, the intercalation of water and the formation of O-functional groups in graphite layers[21] are the causes of the larger *d*-spacing of GO than that of pristine graphite. For the GN/Cu$_{2+1}$O/CF sample, a broad peak at 22.46° (*d*-spacing: 0.395 nm) was found while the peak at 9.5° disappeared which is attributed to the removal of O-functional groups during reduction of GO.[22] And as depicted in Fig. 2, the diffraction peaks at 43.29°, 50.43°, 74.13° which corresponded to the (111), (200) and (220) planes are in accord with Cu (JCPDS no. 04-0836). The diffraction peak at 36.42°, 42.29°, and 61.34° which corresponded to the (111), (200) and (220) plane of Cu$_{2+1}$O (JCPDS no. 05-0667) indicating the partial oxidation Cu. In the obtained hybrid material, Cu$_{2+1}$O (Cu$_2$O with metal excess defects)[23] successfully formed during hydrothermal the process, and Cu foam as 3D conducting scaffold were homogeneously coated by flexible graphene sheets. Fig. 3 shows XPS spectra of the GN/Cu$_{2+1}$O/CF. In the survey region (0−1200 eV), carbon, copper, and oxygen were detected. XPS of Cu 2p of GN/Cu$_{2+1}$O/CF sample was shown in Fig. 3a. Two peaks at 932.2 eV (Cu 2p$_{3/2}$)
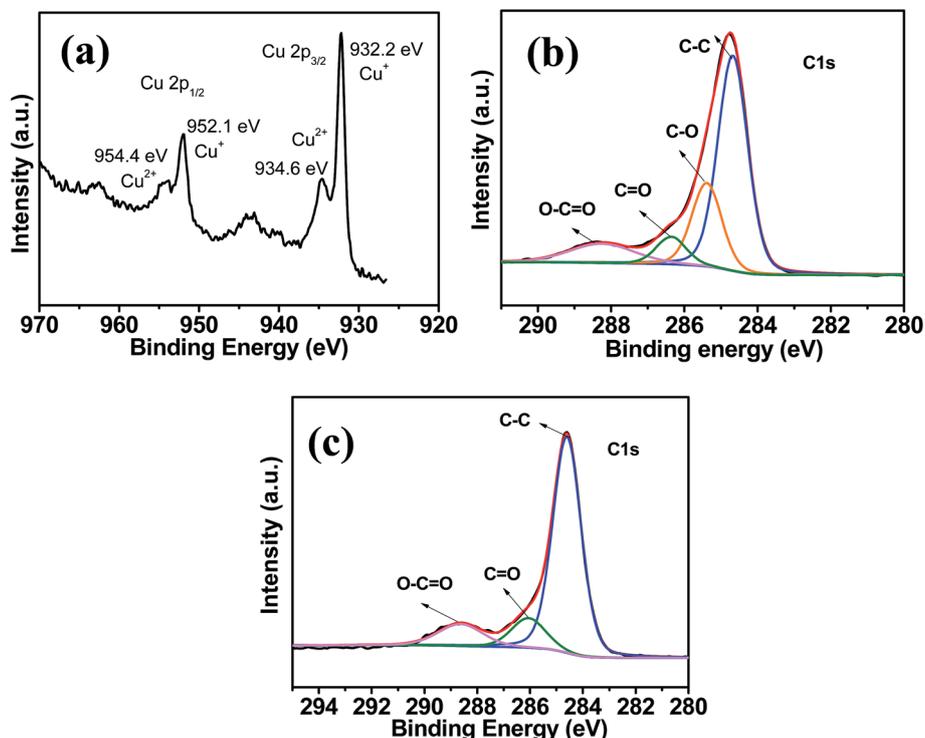

Fig. 3 (a) XPS spectra of Cu and the deconvolutions of (b) C 1s for GO and (c) C 1s XPS for GN/Cu$_{2+1}$O/CF.
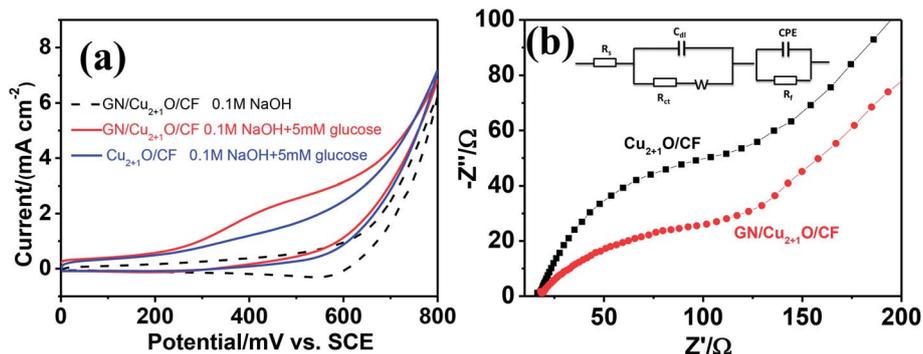
Fig. 4 (a) CVs of GN/Cu$_{2+1}$O/CF electrode in absence of glucose and both Cu$_{2+1}$O/CF and GN/Cu$_{2+1}$O/CF in presence of 5 mM glucose in 0.1 M NaOH at a scan rate of 20 mV s^{-1}. (b) The Nyquist plots of electrodes in 0.1 M NaOH and 5 mM glucose solution.

and 952.1 eV (Cu 2p$_{1/2}$) indicates the Cu$^+$ species on the surface of the sample, and another two peaks with binding energies at 934.6 and 954.4 eV demonstrates the surface of sample containing Cu^{2+} species.[24–27] Deconvolution of the C 1s peak (Fig. 3b) shows four peaks at 284.6 eV (C=C/C–C), 285.4 eV(C–O), 286.4 eV (C=O), and 288.3 eV (O=C–O), corresponding to different functional groups. The C–OH, C=O, and O=C–H peaks indicate the existence of oxygen-containing groups such as hydroxyl, epoxide, and carbonyl in the GO.[28] After the hydrothermal process, from Fig. 3c, the intensities of oxygen-containing peaks decreased, and that of the sp^2-C peak increased indicating that most of oxygen contents in GO were removed and the sp^2-C networks were restored which also demonstrated that the reduction of GO.

Electrochemical performance of the electrodes

Fig. 4a presents the cyclic voltammetry (CV) without (shown in black dotted curve) and with (shown in red and blue curve) the addition of 5 mM glucose in 0.1 M NaOH at a scan rate of 20 mV s^{-1}. Without glucose in alkaline electrolyte, a reduction peak around 600 mV vs. SCE was found which corresponds to the Cu^{2+}/Cu^{3+} redox reaction.[29] After addition of 5 mM glucose, evident enhancement of anodic peak corresponding to the irreversible oxidation of glucose was observed. Although the underlying mechanism during glucose oxidation is currently

unknown, it has been generally considered that the Cu^{3+} species which might be an electron-transfer medium catalyzed glucose oxidation and produced gluconolactone and further hydrolyzed to glucose acid.[30]

The CV measurement of GN/Cu$_{2+1}$O/CF was further performed in presence of glucose at different scan rates. As depicted in Fig. S2,† the peak current densities for the oxidation were linear with the square root of the scan rate, which revealed that the oxidation of glucose at GN/Cu$_{2+1}$O/CF was a diffusion-controlled process.[31] As shown in Fig. S3,† as the glucose concentrations increased, the enhancement of the oxidation current can be observed, and all the peaks for glucose oxidation were between 300 mV and 500 mV vs. SCE, thus, the potential of 450 mV was chosen as applied voltage for amperometric response to optimize the electrocatalytic sensitivity. Fig. 4b shows the impedance spectra of electrodes in 0.1 M NaOH and 5 mM glucose solution, and the Nyquist plots were fitted with the equivalent circuit shown in the inset of Fig. 4b. The Nyquist plots include a half circle at higher frequencies which is related to the charge-transfer resistance and a straight line at lower frequencies corresponds to the diffusion process. The interface electron resistance decreased remarkably suggesting that the introduction of GN into 3D scaffold decreased the interface impedance and accelerated the electron transfer.
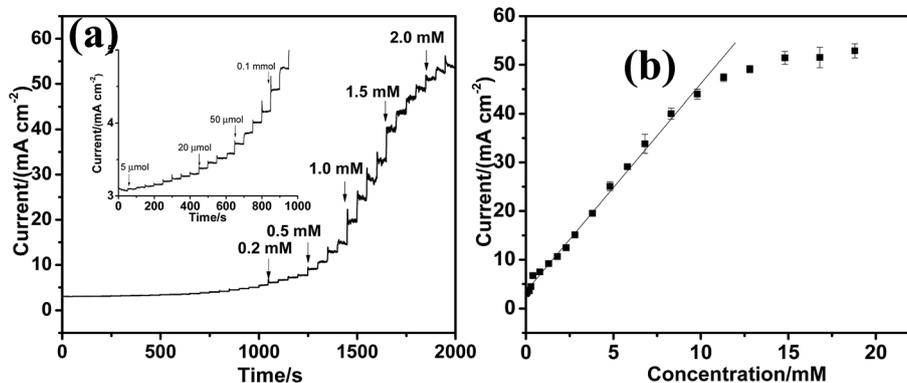

Fig. 5 (a) Amperometric responses of GN/Cu$_{2+1}$O/CF electrode upon successive addition of glucose in 0.1 M KOH at 450 mV (vs. SCE). (b) The corresponding calibration curves of GN/Cu$_{2+1}$O/CF electrode for the glucose detections.

Amperometric response to glucose concentration

The amperometric current responses upon the successive additions of glucose into the alkaline solution are shown in Fig. 5a. After glucose injected, a steady and quick amperometric response can be observed which is attributed to the large surface area and fast electron transfer on $GN/Cu_{2+1}O/CF$ surface. From the calibration curves in Fig. 5b, the $GN/Cu_{2+1}O/CF$ electrode exhibits sensitivity of 3.076 mA mM cm^{-2} which is significantly higher than that of $Cu_{2+1}O/CF$ (Fig. S4†). And the obtained calibration curves are heteroscedastic datas. In addition, Fig. 6a reveals that the detection limit of $GN/Cu_{2+1}O/CF$ was 5 μmol (S/N = 3). Comparison of the performance of electrode with previously reported non-enzymatic glucose sensors is shown in Table S1.† Selectivity is one of the essential parameters of electrochemical nonenzymatic glucose sensing. Coexistence of interferences such as ascorbic acid (AA), chloride species, uric acid (UA), may affect the selectivity of glucose. According to the blood glucose level (3.9–8 mM) and the physiological concentrations of the interfering species, AA and UA (0.1 mM),[32] the selectivity test of the $GN/Cu_{2+1}O/CF$ electrode was conducted by the continuous additions of 1 mM glucose, followed by 0.05 mM of uric acid (UA), 0.05 mM ascorbic acid (AA), 0.1 mM fructose, lactose and 0.1 M sodium chloride in 0.1 M NaOH solution using chronoamperometry at a potential of 450 mV *vs.* SCE. As presented in Fig. 6b, remarkable current enhancement at $GN/Cu_{2+1}O/CF$ electrode can be seen due to the glucose addition, whereas negligible current responses were seen for the interferents. However, as shown in Fig. 6c, the current responses of glucose at CF

Table 1 Detection of glucose in real samples

Sample	Glucometer	Our electrode	RSD (%) $n = 3$
1	5.17	5.2 ± 0.1	3.7
2	4.85	4.9 ± 0.1	4.5
3	6.32	6.4 ± 0.1	3.3

electrode after the additions of interferences reduced evidently. All these indicate that the $GN/Cu_{2+1}O/CF$ electrode showed reliable anti-interference property than that of CF electrode, and it would be suitable for nonenzymatic detection of glucose. As shown in Fig. S5,† the reproducibility was checked by using five $GN/Cu_{2+1}O/CF$ electrodes for detection of 1 mM glucose, and a relative standard deviation (RSD) of 4.60% was obtained. The repeatability of $GN/Cu_{2+1}O/CF$ electrode was also measured with one electrode to detect 1.0 mM glucose four times and a RSD of 1.92% was obtained (Fig. S6†). Stability is another important issue for biosensing. The long-term stability of electrode was tested by recording the current response toward 1 mM glucose for 15 days in air at room temperature. And it is worthy to mention that when used for practical application for glucose detection, the sensor should be better stored in dry and vacuum sealed container to ensure the asepsis and long term stability. In order to avoid cross-contamination in practical applications for glucose monitoring, and due to the low cost of the material used for fabrication the sensor, this kind of enzyme-free glucose sensor is disposable. As displayed in Fig. 6d, the amperometric response is approximately 95.2% of the original value after 15
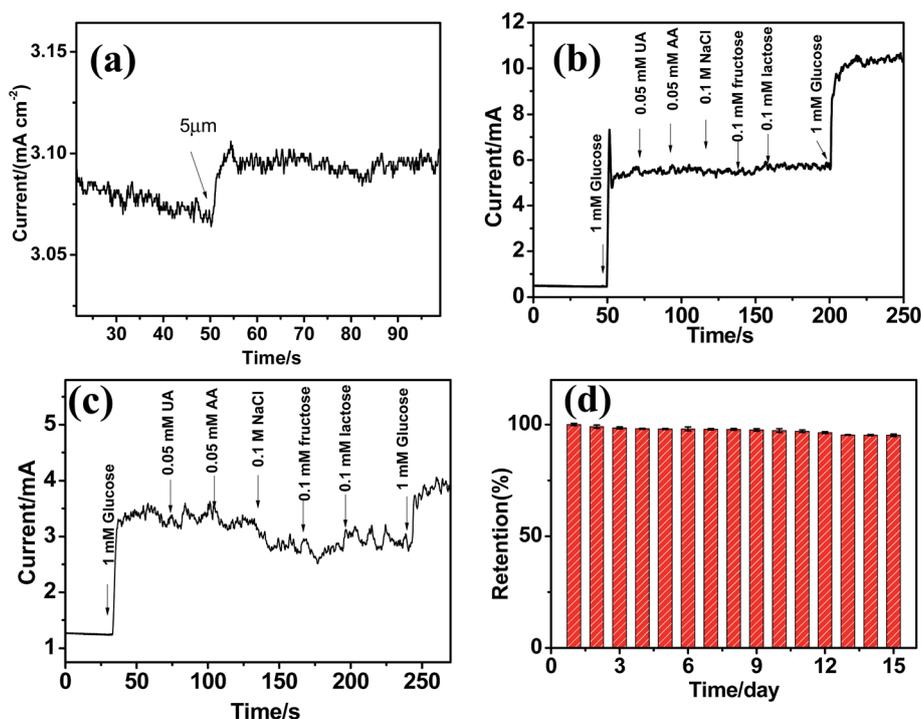

Fig. 6 (a) The amperometric current response for determining detection limit, (S/N = 3). Amperometric response of the (b) $GN/Cu_{2+1}O/CF$ and (c) CF electrode toward the addition of 1 mM glucose and various interfering species in the 0.1 M NaOH solution at 450 mV (*vs.* SCE). (d) Long-term stability of the $GN/Cu_{2+1}O/CF$ electrode over 15 days.

days, suggesting excellent stability of the electrode. In order to evaluate the practical applicability of the sensor, it was employed to detect the concentration of glucose in human serum samples (provided by hospital). 0.01 ml human serum was added into 5 ml 0.1 M NaOH for glucose determine with applied potential of 450 mV. As shown in Table 1, the testing results was in good agreement with the commercial glucose meter, indicating the electrode is practicable for real sample analysis.

Conclusions

In summary, we have successfully demonstrated facile synthesis of GN/Cu$_{2+1}$O/CF *via* a hydrothermal route. The three-dimensional frameworks offers a porous and conductive surface for graphene deposition. And Cu$_{2+1}$O *in situ* grow on the surface of skeletons of the Cu foam coating with GN. Applied in electrocatalysis for glucose detection, the hybrid sensor with large surface area and robust scaffold presents high sensitivity and excellent stability, selectivity and reproducibility and stability which may give a thread for exploring new types of non-enzymatic sensors for glucose sensing.

Acknowledgements

References

1 D. M. Nathan, *J. Am. Med. Assoc.*, 2015, **314**, 1052–1062.

2 S. Chen, H. Zheng, J. Wang, J. Zhou, Q. He, H. Liu, C. Xiong, X. Kong and Z. Nie, *Anal. Chem.*, 2013, **85**, 6646–6652.

3 P. Yang, S. Y. Jin, Q. Z. Xu and S. H. Yu, *Small*, 2013, **9**, 199–204.

4 T. Wen, F. Qu, N. B. Li and H. Q. Luo, *Anal. Chim. Acta*, 2012, **749**, 56–62.

5 J. wang and W. D. Zhang, *Electrochim. Acta*, 2011, **56**, 7510–7516.

6 X. Xu, S. Jiang, Z. Hu and S. Liu, *ACS Nano*, 2010, **4**, 4292–4298.

7 C. Y. Guo, C. Y. Huo, X. Han, C. L. Xu and H. L. Li, *Anal. Chem.*, 2014, **86**, 876–883.

8 X. Y. Zhao, L. L. Fan, Y. Zhang, H. Zhao, X. J. Li, Y. P. Li, L. Wen, Z. F. Yan and Z. Y. Huo, *ACS Appl. Mater. Interfaces*, 2015, **7**, 16802–16812.

9 X. H. Niu, M. B. Lan, H. L. Zhao and C. Chen, *Anal. Chem.*, 2013, **85**, 3561–3569.

10 E. Reitz, W. Z. Jia, M. Gentile, Y. Wang and Y. Lei, *Electroanalysis*, 2008, **20**, 2482–2486.

11 Li. Wang, X. P. Lu, C. J. Wen, Y. Z. Xie, L. F. Miao, S. H. Chen, H. B. Li, P. Li and Y. H. Song, *J. Mater. Chem. A*, 2015, **3**, 608–616.

12 S. D. Sun, X. Z. Zhang, Y. X. Sun, S. C. Yang, X. P. Song and Z. M. Yang, *ACS Appl. Mater. Interfaces*, 2013, **5**, 4429–4437.

13 Z. Z. Li, Y. Chen, Y. M. Xin and Z. H. Zhang, *Sci. Rep.*, 2015, **5**, 16115.

14 M. Zeng and Y. Li, *J. Mater. Chem. A*, 2015, **3**, 14942–14962.

15 X. H. Xiong, D. Ding, D. C. Chen, G. Waller, Y. F. Bu, Z. X. Wang and M. L. Liu, *Nano Energy*, 2015, **11**, 154–161.

16 C. Q. Dong, H. Zhong, T. Y. Kou, J. Frenzel, G. Eggeler and Z. H. Zhang, *ACS Appl. Mater. Interfaces*, 2015, **7**, 20215–20223.

17 M. S. Artiles, C. S. Rout and T. S. Fisher, *Adv. Drug Delivery Rev.*, 2011, **63**, 1352–1360.

18 D. Kuzum, H. Takano, E. Shim, J. C. Reed, H. Juul, A. G. Richardson, J. D. Vries, H. Bink, M. A. Dichter, T. H. Lucas, D. A. Coulter, E. Cubukcu and B. Litt, *Nat. Commun.*, 2014, **5**, 5259.

19 W. S. Hummers and R. E. Offeman, *J. Am. Chem. Soc.*, 1958, **80**, 1339.

20 N. Díez, A. Śliwak, S. Gryglewicz, B. Grzyb and G. Grglewicz, *RSC Adv.*, 2015, **5**, 81831–81837.

21 A. Reina, X. T. Jia, J. Ho, D. Nezich, H. Son, V. Bulovic, M. S. Dresselhaus and J. Kong, Large Area, *Nano Lett.*, 2009, **9**, 30–35.

22 Y. D. Lei, Z. H. Tang, R. J. Liao and B. C. Guo, *Green Chem.*, 2011, **13**, 1655–1658.

23 L. L. Tian, X. Y. Wei, Q. C. Zhuang, Z. M. Zong and S. G. Sun, *Acta Chim. Sin.*, 2013, **71**, 1270–1274.

24 Y. K. Hsu, C. H. Yu, Y. C. Chen and Y. G. Lin, *RSC Adv.*, 2012, **2**, 12455–12459.

25 L. Peng, J. Zhang, J. Li, B. Han, Z. Xue and G. Yang, *Chem. Commun.*, 2012, **48**, 8688–8690.

26 M. Hanke, H. K. Arslan, S. Bauer, O. Zybaylo, C. Christophis, H. Gliemann, A. Rosenhahn and C. Wöll, *Langmuir*, 2012, **28**, 6877–6884.

27 M. C. Biesinger, L. W. M. Lau, A. R. Gerson and R. S. C. Smart, *Appl. Surf. Sci.*, 2010, **257**, 887–898.

28 J. W. Lee, A. S. Hall, J. D. Kim and T. E. Mallouk, *Chem. Mater.*, 2012, **24**, 1158–1164.

29 S. K. Meher and G. R. Rao, *Nanoscale*, 2013, **5**, 2089–2099.

30 M. Marioli and T. Kuwana, *Electrochim. Acta*, 1992, **37**, 1187–1197.

31 S. Felix, P. Kollu, B. Raghupathy, S. K. Jeong and A. N. Grace, *J. Chem. Sci.*, 2014, **126**, 25–32.

32 B. Liu, R. Hu and J. Deng, *Anal. Chem.*, 1997, **69**, 2343–2348.